J Physiol Sci (2017) 67:151–162
DOI 10.1007/s12576-016-0449-0

ORIGINAL PAPER

Expression of the TRPM6 in mouse placental trophoblasts; potential role in maternal–fetal calcium transport

Yoshiro Suzuki[1,2] · Masaki Watanabe[1,3] · Claire T. Saito[1] · Makoto Tominaga[1,2]

Received: 20 January 2016 / Accepted: 20 March 2016 / Published online: 4 April 2016

Abstract The placenta is required to transport calcium (Ca^{2+}) from mother to fetus during fetal bone mineralization. In an attempt to clarify the molecular basis of Ca^{2+} entry for this transport, we identified TRPM6 as a candidate for apical Ca^{2+} entry pathway. TRPM6 mRNA increased during the last 4 days of pregnancy, coinciding with fetal bone mineralization in mice. TRPM6 mRNA and protein was localized in the trophoblasts in labyrinth where the maternal–fetal Ca^{2+} transport occurs. In patch-clamp recordings, we observed TRPM6/TRPM7-like currents in mouse trophoblasts after starting fetal bone mineralization but not before mineralization. Plasma membrane Ca^{2+} permeability was significantly increased in TRPM6/TRPM7 expressed HEK293 cells under physiological Mg^{2+} and ATP concentration but not in TRPM6 or TRPM7 homomer-expressing cells. These results suggest that TRPM6 is functionally expressed in mouse placental trophoblasts, implicating in maternal–fetal Ca^{2+} transport likely with TRPM7, which might enable to sustain fetal bone mineralization.

Keywords TRPM6 · TRPM7 · Maternal–fetal calcium transport · Placenta · Trophoblasts

Introduction

Calcium (Ca^{2+}) has essential roles in fetal growth and development. Fetal blood Ca^{2+} concentration is maintained for the function and development of excitatory cells including the nervous system and heart, as well as other non-excitable cells. In parallel, Ca^{2+} is used for fetal bone mineralization. Many reports have shown that fetal blood Ca^{2+} levels are higher than maternal levels when fetal bones are mineralized [1–3]. These indicate that Ca^{2+} is actively transported from mother to fetus via the placenta in late pregnancy. However, the molecular mechanism and the regulation of the maternal–fetal Ca^{2+} transport remains unclear.

In the placenta, trophoblasts play the main role in maternal–fetal nutrient transport including Ca^{2+}. In the placenta during late pregnancy, Ca^{2+} is thought to be transported through a transcellular pathway rather than a paracellular route due to the uphill nature of the Ca^{2+} gradient. There are three molecular processes involved in the transcellular pathway: (1) Ca^{2+} enters into the cell using an electrochemical gradient likely through Ca^{2+}-permeable cation channels; (2) Ca^{2+} binds to calbindin D_{9K}, an intracellular Ca^{2+} buffer to avoid an increase of the intracellular free Ca^{2+} concentration; (3) Ca^{2+} is extruded mainly via plasma membrane Ca^{2+}-ATPase (PMCA) [4, 5]. Among these processes, it is not yet clear which Ca^{2+} channel is responsible for the Ca^{2+} entry

Electronic supplementary material The online version of this article (doi:10.1007/s12576-016-0449-0) contains supplementary material, which is available to authorized users.

✉ Yoshiro Suzuki
yoshiro@nips.ac.jp

✉ Makoto Tominaga
tominaga@nips.ac.jp

[1] Division of Cell Signaling, Okazaki Institute for Integrative Bioscience (National Institute for Physiological Sciences), National Institutes of Natural Sciences, Okazaki 444-8787, Japan

[2] Department of Physiological Sciences, SOKENDAI (The Graduate University for Advanced Studies), Okazaki 444-8787, Japan

[3] Department of Renal and Urologic Surgery, Asahikawa Medical University, Asahikawa 078-8510, Japan

process. In a previous study, the TRPV6 (transient receptor potential vanilloid 6) knockout mouse exhibited a decrease in maternal–fetal Ca^{2+} transport [6]. However, the majority of Ca^{2+} transport was still remained in these mice. This result suggested that there is another key factor for the Ca^{2+} entry pathway. In this study, we focused on TRPM6 (transient receptor potential melastatin 6) as another candidate for this pathway. The expression pattern of TRPM6 in mouse placenta was temporally and spatially consistent with such a role. Membrane current and Ca^{2+}-permeability assays under physiological conditions suggested the presence of endogenous TRPM6-derived Ca^{2+}-entry in mouse placental trophoblasts. These suggest that TRPM6 contributes to the Ca^{2+} entry for the maternal–fetal Ca^{2+} transport.

Materials and methods

Animals

All animal experiments were performed with C57BL/6NCr pregnant mice (SLC Japan). All procedures were conducted in accordance with the policies of the Institutional Animal Care and Use Committee, National Institute for Physiological Sciences.

Molecular cloning of mouse TRPM6 and TRPM7 cDNA

Mouse kidney cDNA was synthesized using the Superscript III kit (Life Technologies Corporation, Carlsbad, CA, USA) and poly-A-rich RNA from mouse kidney (Takara, Japan). PCR reactions with mouse TRPM6 or TRPM7-specific primers were performed with 10 µl of 5× Phusion HF buffer, 4 µl dNTPs (2.5 mM), 1 µl mouse kidney cDNA, and 0.5 µl Phusion DNA polymerase (Thermo Fisher Scientific, Waltham, MA, USA), using the following temperature cycles: 98 °C for 30 s, then ten cycles of 98 °C for 10 s, 68 °C for 3 min, and 72 °C for 3 min, then 30 cycles of 98 °C for 10 s and 72 °C for 3 min. After elongation at 72 °C for 10 min, PCR products were purified using a gel extraction kit (Takara, Japan) from 0.7 % agarose gel electrophoresis and used as template for secondary PCR; 10 µl of 5× Phusion HF buffer, 4 µl dNTPs, mouse TRPM6 or TRPM7-specific primers, purified PCR fragments, and 0.5 µl of Phusion DNA polymerase. The cycles for secondary PCR were as follows: 98 °C for 30 s, then 30 cycles at 98 °C for 10 s and 72 °C for 3 min, then elongation at 72 °C for 10 min. The secondary PCR products were again purified, and introduced into the pcDNA3.1 vector (Life Technologies) after digestion using Bam *H*I and Not I (NEB, USA). Sequences were confirmed using a DNA sequence analyzer (ABI, USA). The GenBank accession numbers are as follows; mouse TRPM6 (NM_153417), mouse TRPM7 (NM_021450).

RT-PCR

Whole placenta from pregnant mouse at 14 or 18 days post-fertilization were resected from anesthetized mice. Total RNA was isolated using a Sepasol I kit (Nacalai, Japan). First-strand cDNA was synthesized using a Revertra Ace kit (Toyobo, Japan). Conventional polymerase chain reaction (PCR) was performed using rTaq polymerase (Takara, Japan) with specific primer sets for all mouse TRPMs, TRPVs, and TRPA1 (Table S1). The PCR products were visualized by agarose gel electrophoresis with 2 % agarose (Ultrapure agarose, Life Technologies, USA). Plasmid with partial cDNA fragment of each TRP channels was used to verify PCR reactions. GAPDH was used as a housekeeping gene.

Quantitative PCR

Quantitative PCR analysis was performed using a StepOne analyzer (Life Technologies, USA) as described previously [7]. The temperature profile consisted of 40 cycles of denaturation (95 °C, 15 s), annealing (60 °C, 30 s), and elongation (72 °C, 1 min). Melting curve analysis was performed at the end of each assay to discriminate specific from non-specific signal. To quantify the amount of cDNA, purified PCR products with known concentration were serially diluted and used as standards. The ΔΔCt method was applied to compare the expression levels from each time point. Beta-actin was used as a housekeeping gene. The expression level of β-actin was consistent between gestational ages.

In situ hybridization

In situ hybridization was performed as described previously [6, 8]. The placenta, along with the extraplacental yolk sac, was resected from anesthetized mice at 18 days post-fertilization. The tissue was frozen with OCT compound (Sakura, Japan), cut using a cryostat (CM3050S, Leica, Germany) at −20 °C with 20-µm thickness. Sections were incubated in PBS with 4 % paraformaldehyde (PFA) for 2 h at room temperature and washed twice with 2 × SSC. The sections were then treated with Tris–EDTA containing 5 µg/ml of proteinase K at 37 °C for 15 min with stirring. Those sections were incubated with 4 % PFA again, washed twice with 2 × SSC, and incubated with 0.1 M triethanolamine solution (pH 8.0) with 0.5 % acetic anhydride for 10 min at room temperature with stirring. After washing with Milli-Q water and treated with

hybridization solution (50 % deionized formamide, 4 × SSC, 2 × Denhardt's solution) at 50 °C for 2 h, sections were treated with the same hybridization buffer containing 1 % dextran sulfate and a denatured, digoxigenin-labeled RNA probe at 50 °C overnight in a humidified chamber. Sections were washed with 2 × SSC with 50 % formamide for 30 min at 37 °C with stirring, then treated with 2 × SSC with 1 U/ml RNase T1 (Roche, Switzerland) for 30 min at 37 °C with stirring. Next, sections were washed twice with 2 × SSC, 0.1 % SDS for 10 min at 55 °C, and twice with 0.2 × SSC, 0.1 % SDS for 10 min at 55 °C. After incubation with 1 % blocking reagent in maleic acid buffer (Roche, Switzerland), sections were treated with anti-digoxigenin-AP Fab fragments (1:1000, Roche, Switzerland) in the blocking solution for 2 h at room temperature in a humidified chamber. Sections were washed twice with maleic acid buffer with 0.2 % Tween-20 for 10 min with stirring, equilibrated in ALP detection buffer (0.1 M Tris–HCl, pH 9.5, 0.1 M NaCl, 50 mM $MgCl_2$), and incubated in a substrate solution (Roche, Switzerland) with polyvinyl alcohol and levamisole at 30 °C overnight. After washing, sections were mounted with Fluoromount (Diagnostic BioSystems, USA).

Sense and antisense RNA probes were synthesized from plasmid containing mouse TRPM6 cDNA inserted into pCR2.1 (Life Technologies) using a digoxigenin RNA labeling kit (Roche, Switzerland). Plasmid containing mouse TRPM6 cDNA was linearized and cRNA probes were synthesized in vitro from fragments containing 472 bp of TRPM6 (nt. 1958-2430, NM_153417). The digoxigenin labeling was confirmed by dot-blot experiments.

Western blotting

Human embryonic kidney-derived 293T cells (HEK293T) were maintained in DMEM with 10 % heat-inactivated FBS, 100 units/ml penicillin and streptomycin, 2 mM L-glutamine, and 5 % CO_2 at 37 °C. HEK293T cells were transfected with the appropriate plasmids using Lipofectamine reagent (Life Technologies). To prevent Ca^{2+} overload into the cells through TRPM6/TRPM7 heteromers, ruthenium red (2 μM) was added into the medium just after the transfection and compared with cells without ruthenium red treatment. After 18-h incubation, cells were washed with ice-cold PBS and lysed in 500 μl TNE buffer (10 mM Tris–HCl, pH 7.4, 150 mM NaCl, 1 mM EDTA, 1 mM Na_3VO_4) with protease inhibitors (Complete, Roche) and 1 % NP-40. After homogenizing, proteins were centrifuged at 10,000 × *g* for 60 min at 4 °C. Supernatant (membrane fraction) was quantified and kept at −20 °C until use. SDS-PAGE was performed with the protein sample (2 μg) in 7.5 % polyacrylamide gel, and then transferred into a PVDF membrane. The membrane was blocked overnight at 4 °C with 3 % BSA in PBS-T and then incubated with rabbit anti-mouse TRPM6 antibody (Alomone Labs, 1/300 dilution in 3 % BSA in PBS-T) with or without antigen peptides. After three washes with PBS-T, the membrane was incubated with anti-rabbit IgG HRP (CST, 1/3000 dilution) for 30 min at room temperature, then signal was visualized by ECL prime kit (Amersham) and FLA3000mini (Fujifilm).

Immunohistochemistry

Immunohistochemistry was performed as described previously [9]. Pregnant mice at 18 days post-fertilization were anesthetized and the placenta was resected. The tissue was frozen with OCT compound (Sakura, Japan) and stored at −80 °C until use. Sections (8 μm) were cut by a cryostat (CM3050S, Leica, Germany), fixed with 10 % buffered formaldehyde for 10 min at room temperature. After washing with PBS 3 times, sections were incubated with 5 % normal goat serum with 0.05 % Triton X-100 (Sigma, USA) at 4 °C overnight for blocking. Sections were treated at 4 °C overnight with primary antibody; rabbit anti-mouse TRPM6 (Alomone Labs, Israel) with 1/50 dilution. After washing three times with PBS containing 0.05 % Triton X-100, sections were incubated with secondary antibody (Alexa488, Molecular Probes, Eugene, Oregon, USA) with 1/100 dilution for 90 min at room temperature. After washing three times with PBS containing 0.05 % Triton X-100, sections were mounted with Fluoromout (DBS, USA) and analyzed by using a fluorescent microscope (BZ-9000, Keyence, Japan).

Isolation of mouse primary trophoblasts

Mouse primary trophoblasts were isolated as described previously with some modifications [10]. Pregnant mice (C57BL/6NCr, 14 or 18 days post-fertilization) were anesthetized and the placenta was dissected. The tissue was cut into pieces using scissors and incubated in Medium 199 (Life Technologies) containing 1 mg/ml collagenase (Sigma, USA) with 20 μg/ml DNase (Life Technologies) at 37 °C for 1 h with shaking. After the collagenase treatment, cells were mixed by pipetting (P1000, Gilson, France) 30 times, filtered with a 250 μm followed by 60-μm filter. After washing with NCTC-109 (Life Technologies), primary trophoblasts were cultured with NCTC-109 containing Glutamax, 1.65 mM cysteine, 10 % fetal bovine serum, and penicillin/streptomycin (Life Technologies) until use (from 5 to 10 h for patch-clamp recording, 18–24 h for Ca^{2+} imaging). Culture dishes were coated with poly-L-lysine (Sigma) before use.

Measurement of intracellular Ca^{2+} concentrations

Primary cultures of mouse trophoblasts or HEK293T cells were loaded with the fluorescent Ca^{2+} indicator Fura-2 (5 μM, Fura-2-acetoxymethyl ester, Life Technologies) in NCTC-109 medium (trophoblasts) or DMEM medium (HEK293T) at 37 °C. Cytosolic Ca^{2+} concentrations were measured in a standard bath solution containing 150 mM NaCl, 5 mM KCl, 1.8 mM $CaCl_2$, 1.2 mM $MgCl_2$, 25 mM HEPES (pH 7.4 adjusted with NaOH), and 10 mM glucose; ratiometric imaging was performed with Fura-2 at 340 and 380 nm, and the emitted light signal was read at 510 nm with a CCD camera (CoolSnap ES, Roper Scientific/Photometrics, Fairfax, USA). The ratio of F340/F380 was calculated and acquired with an imaging processing system (IP-Lab, Scanalytics Inc., USA) and ImageJ (https://imagej.nih.gov/ij/). Changes in the delta ratio were calculated by subtracting basal values from peak values, and all the values were normalized with that of ionomycin (5 μM, Sigma, USA).

Plasma membrane Ca^{2+} permeability was estimated by calculating an increase in intracellular Ca^{2+} concentration after extracellular Ca^{2+} application [11]. Initial Ca^{2+} levels were measured before the application. Basal Ca^{2+} levels were determined when cells were treated with 2 mM EDTA solution without Ca^{2+}. Next, solution containing 2 mM Ca^{2+} was superfused. An intracellular Ca^{2+} increase, which was an indicator of plasma membrane Ca^{2+} permeability, was determined and normalized with that of ionomycin value.

Whole-cell patch-clamp recording

Whole-cell patch-clamp recordings were carried out as described previously with some modifications [9]. Mouse primary trophoblasts derived from pregnant mouse at 14 or 18 days after fertilization were maintained in NCTC-109 medium until recording (for 3–8 h). Human embryonic kidney-derived 293 (HEK293) T cells were transfected with 1.0 μg of empty vector pcDNA3.1 (mock), mouse TRPM6, TRPM7, or both TRPM6 and TRPM7 (each 0.5 μg), using Lipofectamine Plus Reagent (Life Technologies). Whole-cell patch-clamp recordings were performed 6–10 h after starting the culture (trophoblasts) or 14–24 h after transfection (HEK293T). Standard bath solution for TRPM6/7 contained 130 mM NaCl, 5 mM KCl, 10 mM HEPES, pH 7.4, 1 mM $MgCl_2$, 2 mM $CaCl_2$, 27 mM mannitol. The pipette solution contained 100 mM Cs aspartate, 20 mM CsCl, 2.93 mM $CaCl_2$, 10 mM HEPES, pH 7.4, 4 mM Na_2ATP, and 10 mM BAPTA. Data were sampled at 10 kHz and filtered at 4 kHz for analysis using an Axon 700B amplifier with pCLAMP software (Axon Instruments, USA). Membrane potential was clamped at -60 mV, and voltage ramp-pulses from −110 mV to +110 mV (400 ms) were applied every 5 s. All experiments were performed at room temperature.

Statistical analysis

Data are represented as the mean ± SEM. Statistical analysis was performed using the Student's *t* test, or one-way ANOVA with Bonferroni's post hoc test. Differences with *p* values of less than 0.05 were considered significant.

Results

TRPM6 as a candidate Ca^{2+} entry channel of placental trophoblasts

In an attempt to clarify the molecular basis of maternal–fetal Ca^{2+} transport during fetal bone mineralization, we focused on TRP channels, since it had been reported that ruthenium red, a broad TRP channel blocker inhibits Ca^{2+} uptake activity in placental trophoblasts [12]. To determine which TRP channel is involved, we first examined the expression levels in mice of all TRPV, TRPM, and TRPA channels in mouse placenta at 14 or 18 days post-fertilization (before or after initiation of fetal bone mineralization [13], Fig. S1). Among these TRP channels, we found that the expression of TRPM6 mRNA significantly increased ($p < 0.01$, $n = 7$, Student's *t* test) (Fig. 1a). In contrast, expression level of TRPM7 mRNA was not significantly changed (Fig. 1b). TRPV6 was found to be expressed and increased as previously described [6] (Fig. S1). In this study, we focus on TRPM6 for further analysis.

Localization of TRPM6 in mouse placenta

We performed in situ hybridization in mouse placenta at 18 days post-fertilization to investigate the localization of TRPM6 mRNA. As a positive control, we used antisense probe of β-actin, which stained almost all the cells in the placenta (Fig. 1c), whereas a staining without DIG-labeled probes did not show any significant signal (Fig. 1d). TRPM6 mRNA was mainly localized in the labyrinthine trophoblasts (Fig. 1e, g). These signals were not observed when we used sense probe (Fig. 1f, h). We also performed immunohistochemistry and Western blotting to determine the protein expression of TRPM6 in the placenta at 18 days post-fertilization. In Western blotting, we observed a ~230-kDa band, which was decreased under antigen treatment (Fig. 2a; lane 3, Fig. 2b; lane 3, theoretical molecular weight of mouse TRPM6 is 233 kDa) but not in mock transfected HEK293T cells (lane 2). However, we

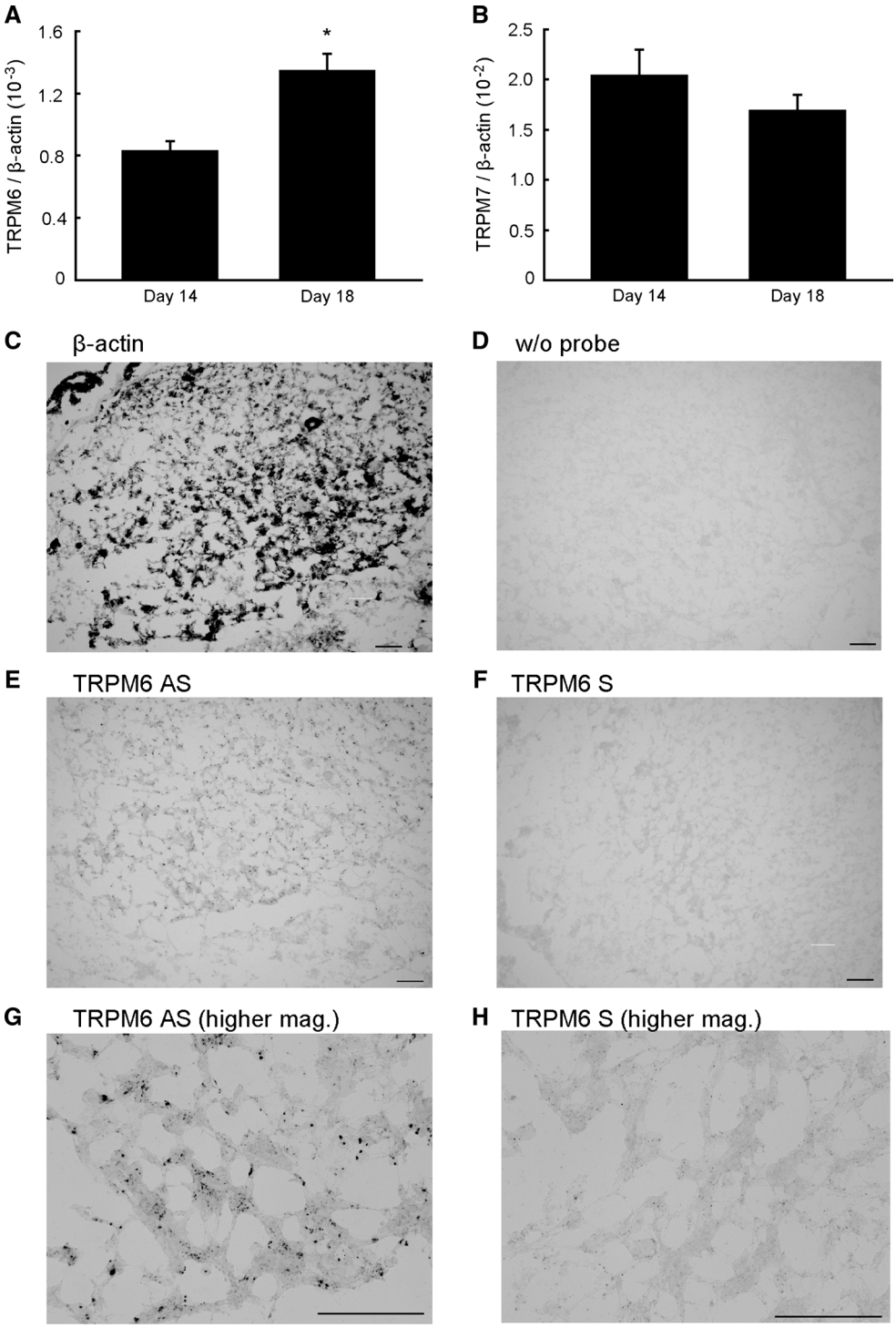

Fig. 1 TRPM6 mRNA expression in mouse placenta: **a**, **b** quantitative PCR of TRPM6 or TRPM7 in mouse placenta at 14 or 18 day post-fertilization. The increase of TRPM6 mRNA was statistically significant ($p < 0.01$, $n = 7$, **a**), whereas TRPM7 mRNA level was not significantly changed during development ($n = 7$, **b**). **c**–**h** In situ hybridization of β-actin or TRPM6 in mouse placenta at 18 days post-fertilization. Labyrinthine trophoblasts were labeled by TRPM6 antisense probe ($n = 5$, **e**, **g**) but not by sense probe (**f**, **h**). Almost all the cells were stained by antisense probe of β-actin (**c**). No significant staining was observed in a negative control without DIG-labeled probes (**d**). *Scale bars* 100 μm

could not get clear band in cells expressing TRPM6 and TRPM7 (lane 4). We hypothesized that this was because of the Ca^{2+} overload through these overexpressed TRPM6/TRPM7 heteromers, and cells might be dead as reported previously in the case of TRPV5 mutants whose intracellular Ca^{2+}-dependent inactivation was impaired [14]. Indeed, when we added ruthenium red (2 μM) in the medium after transfection to prevent Ca^{2+} overload through overexpressed TRPM6/TRPM7 heteromers, we could observe strong band in cells overexpressing TRPM6 and TRPM7 (lane 7). We could also observe a strong band in TRPM6-expressing cells, probably because of the partial heteromer formation of TRPM6 with endogenously expressing TRPM7 in HEK293T cells (lane 6). In

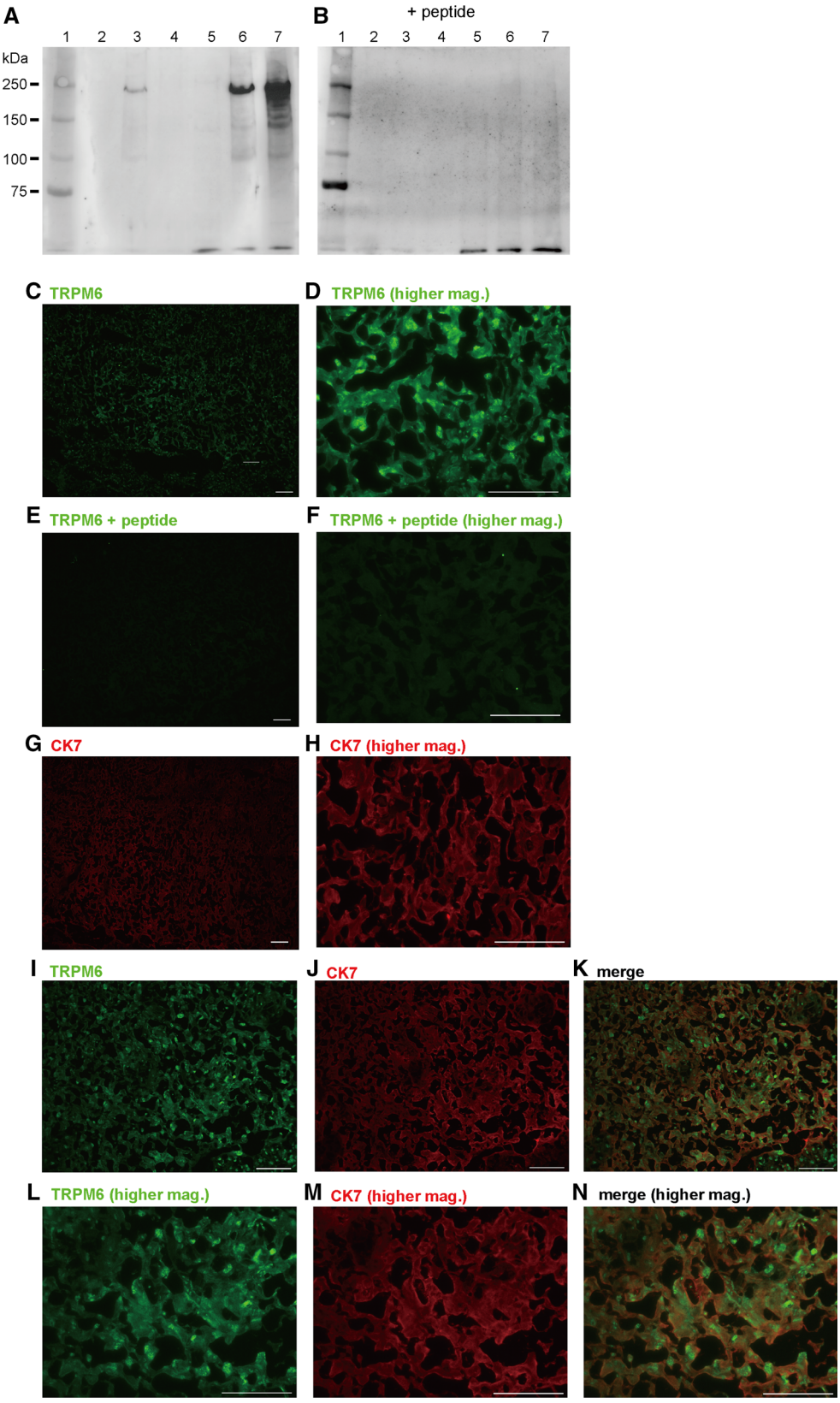

Fig. 2 TRPM6 protein expression in mouse placenta: **a**, **b** Western blotting of TRPM6 in HEK293T cells exogenously expressed mock transfected (*lanes 2* and *5*), or exogenously expressing TRPM6 (*lanes 3* and *6*), TRPM6 with TRPM7 (*lanes 4* and *7*), under the absence (*lanes 2–4*) or presence (*lanes 5–7*) of ruthenium red (2 μM). When TRPM6 was co-expressed with TRPM7, a strong signal was observed around 230 kDa in the presence of ruthenium red (*lane 7*), which was absent under the antigen peptide treatment (**b**). *Lane 1* shows a molecular weight marker. **c**–**n** Immunohistochemistry of TRPM6 (**c**, **d**) or CK7 (**g**, **h**) in mouse placenta. TRPM6 protein signals (*green*) at 18 days post-fertilization were colocalized with CK7 (*red*) (**i**–**n**). This signal was absent under the antigen treatment in the absorption assay (**e**, **f**). *Bars* 100 μm

immunohistochemistry, we used cytokeratin 7 (CK7) as a marker for trophoblasts (Fig. 2g, h). Although strong signals were seen in the nucleus, which were most likely false positives, TRPM6 signals were observed at the plasma membrane and cytosol in trophoblasts in labyrinth, colocalizing with CK7 (Fig. 2c, d, i–n). These signals were also seen in trophoblasts in other regions but expression levels were smaller compared to labyrinth. This observation was comparable to the result of in situ hybridization (Fig. 1e, g). Moreover, TRPM6 signals were decreased under the antigen treatment in antibody absorption tests (Fig. 2e, f). These results strongly suggest that TRPM6 is expressed in trophoblasts.

Ca^{2+} permeability in mouse primary trophoblasts and HEK293T cells

Our next question was the functional significance of TRPM6 in mouse placenta. For this purpose, we cultured mouse primary trophoblasts [10]. In our culture condition, RT-PCR experiments indicated that placental lactogen II (a marker for placental trophoblasts), TRPM6 and TRPM7 were positive, but no signals were detected for TRPV1 or TRPV3 (Fig. 3a). These results suggest that the majority of these primary cells are trophoblasts. By using these primary cells, we measured plasma membrane Ca^{2+} permeability using the Ca^{2+} indicator Fura-2 [11]. We used 2-aminoethoxydiphenyl borate (2-APB) with various concentrations to discriminate activities derived from TRPM6, TRPM7, TRPM6/TRPM7 heteromers, or other channels such as TRPV2 or TRPV6. These channels have been reportedly activated or inhibited by 2-APB with different EC_{50}/IC_{50} values. For example, TRPM6 is activated by 2-APB with an EC_{50} value of 205 ± 10 μM [15]. On the other hand, TRPM7 is inhibited with an IC_{50} value of 178 ± 14 μM [15]. The Ca^{2+} permeability of our primary culture cells was significantly higher with application of 2 mM 2-APB ($p < 0.05$, $n = 11$–12, Student's t test, Fig. 3b–d) but not in lower concentrations, suggesting that the Ca^{2+} permeability was mediated by TRPM6/TRPM7 heteromer, whose reported EC_{50} value was 1.6 ± 0.1 mM [15]. There might be a small contribution of TRPV2 ($EC_{50} = 22$ μM) [16], or TRPV6 (2-APB inhibits TRPV6, $IC_{50} = 68.66$ μM) [17]. Indeed, the expression level of

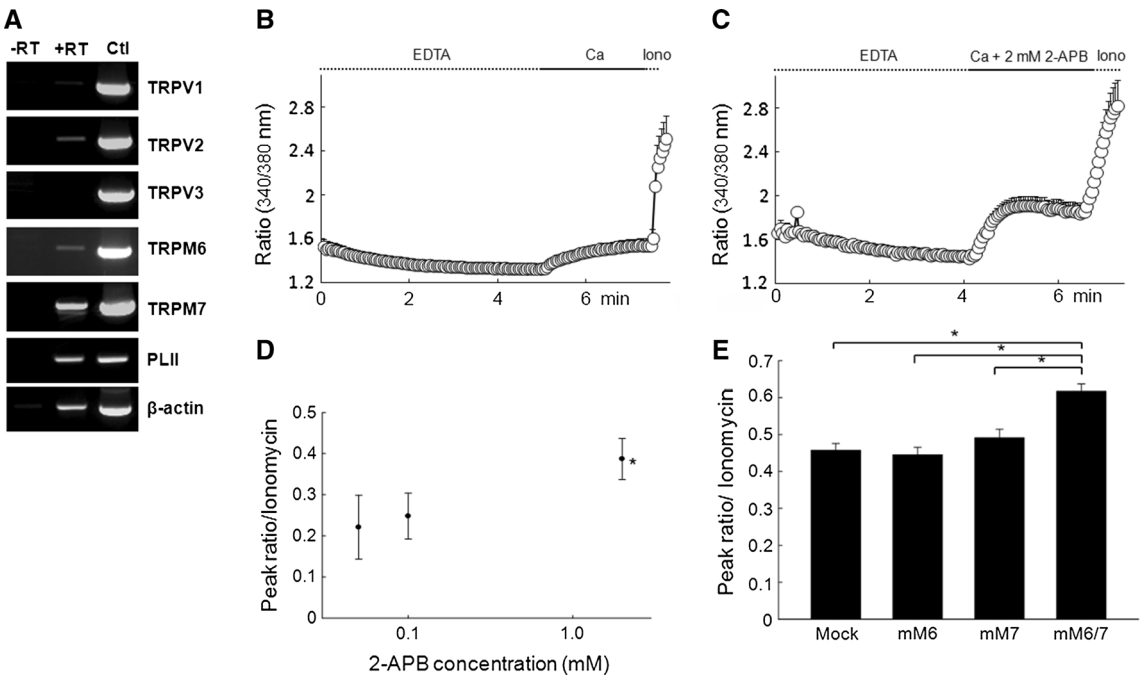

Fig. 3 Measurement of intracellular Ca^{2+} concentration before and after application of extracellular Ca^{2+}: **a** RT-PCR in isolated mouse trophoblasts from placenta at 18 days post-fertilization. The strong placental lactogen II signal suggested that this included a trophoblast-rich population. TRPM6 as well as TRPM7 were expressed in these cells. Control means PCR reaction using plasmid of partial TRP channel cDNA as a template. **b**, **c** Time traces of intracellular Ca^{2+} concentration before and after extracellular EDTA (2 mM) treatment in mouse primary trophoblasts. The Ca^{2+} increase after application of 2 mM Ca^{2+} represents plasma membrane Ca^{2+} permeability. Co-application of 2-APB (2 mM) significantly increased the Ca^{2+} permeability ($n = 12$, **c**, **d**) but lower concentrations (50 and 100 μM, **d**) did not ($n = 12$), suggesting a contribution of the TRPM6/TRPM7 heteromers to the Ca^{2+} permeability in primary trophoblasts. **e** Plasma membrane Ca^{2+} permeability in mock-transfected HEK293T cells or HEK293T cells expressing TRPM6, TRPM7, or TRPM6 with TRPM7. The Ca^{2+} permeability of TRPM6 with TRPM7 was statistically higher compared to the mock-transfected cells ($p < 0.001$, $n = 20$, Student's t test), but not in the cell transfecting TRPM6 or TRPM7 alone

TRPV2 mRNA was not changed much between 14 and 18 days post-fertilization (Fig. S1). Furthermore, TRPV2 activator lysophosphatidyl choline (LPC, 30 μM) did not increase the Ca^{2+} uptake, which supports the idea that the contribution of TRPV2 was small (data not shown).

It has been reported that TRPM6/TRPM7 heteromer exhibits channel activity under physiological concentrations of intracellular Mg^{2+} and ATP, but TRPM6 homomer and TRPM7 homomer do not, since homomers of TRPM6 or TRPM7 are blocked by physiological concentration of extracellular and intracellular Mg^{2+} [18]. To confirm this, we investigated plasma membrane Ca^{2+} permeability in a HEK293T cells expressing these channels [11]. Actually, Ca^{2+} permeability was significantly higher compared to the mock-transfected control when TRPM6 was co-expressed with TRPM7 ($p < 0.001$, $n = 20$, Student's t test), but not with TRPM6 or TRPM7 alone (Fig. 3e). We assumed that TRPM6/TRPM7-expressing cells should have higher intracellular Ca^{2+} concentration in a steady-state condition as well because extracellular solution contained 2 mM Ca^{2+}. We also compared the Fura-2 ratios in these cells in a steady state. However, we could not detect a significant difference between these cells (data not shown).

Patch-clamp recordings in mouse primary trophoblasts

We performed whole-cell patch-clamp experiments in mouse primary trophoblasts to confirm the functional significance of TRPM6/TRPM7 heteromer. We used intracellular and extracellular divalent cation-free conditions to enhance TRPM7-like currents. At 14 days post-fertilization, we observed Mg^{2+}-inhibitable outwardly rectifying currents, which were significantly inhibited by 0.1 mM 2-APB ($p = 0.025$, one-way ANOVA with Bonferroni post hoc test, $n = 7$, Fig. 4a, c). This suggests that these currents were mediated by TRPM7 homomer [15]. We did not observe TRPV2-like currents (EC_{50} for 2-APB is 22 μM), again supporting the supposition that there was a small contribution of TRPV2 in mouse placental trophoblasts, at least in our condition. We also observed a fast inhibition and slow activation kinetics of 2-APB with higher concentrations (2 mM, Fig. 4a) as previously reported in cloned mouse TRPM7 [15]. For statistics, we used the values at the fast inhibition phase. In contrast, 2-APB-inhibitable currents were not observed at 18 days post-fertilization. Membrane currents were even activated significantly by 0.5 mM 2-APB ($p = 0.047$, $n = 5$, one-way ANOVA with Bonferroni post hoc test, Fig. 4b, c) as previously reported in the TRPM6/TRPM7-coexpressing cells [15].

Patch-clamp recordings in TRPM6 and TRPM7 expressing HEK293T cells

We cloned mouse TRPM6 and TRPM7 cDNAs to perform whole-cell patch-clamp recording in HEK293T cells. Figure 5 shows representative time traces of membrane currents from mock (a), TRPM7 alone (b), and combined TRPM6 and TRPM7 (c) transfected HEK293T cells. We did not observe any differences between mock and TRPM6 (data not shown), as previously reported [18, 19]. Indeed, in our hands, TRPM7 currents showed almost the same 2-APB responses (Fig. 5b, d) as observed in trophoblasts at 14 days post-fertilization (Fig. 4a, c); 2-APB (0.1 mM) inhibited those currents ($p = 0.002$, $n = 7$, one-way ANOVA with Bonferroni post hoc test) and higher concentration (2 mM) exhibited the fast-inhibition and slow-activation kinetics. When TRPM6 was expressed with TRPM7, currents showed similar 2-APB responses (Fig. 5c, d) as observed in trophoblasts at 18 days post-fertilization (Fig. 4b, c); 2-APB (0.5 mM) activated those currents ($p = 0.013$, $n = 4$, one-way ANOVA with Bonferroni post hoc test).

Discussion

In this study, we focused on TRPM6, a Ca^{2+}-permeable cation channel. Our finding is that (1) TRPM6 mRNA and protein are localized in the labyrinthine trophoblasts, which have been reported to be important for the maternal–fetal Ca^{2+} transport. (2) The TRPM6 expression increased coinciding with fetal bone mineralization. (3) We observed endogenous TRPM6/TRPM7-like currents and intracellular Ca^{2+} increases likely through endogenous TRPM6/TRPM7 in mouse placental trophoblasts from 18 days, but not from 14 days post-fertilization. These results suggest that TRPM6 is functionally expressed in mouse placental trophoblasts playing a role in Ca^{2+} transport from mother to fetus in order to sustain fetal bone mineralization.

However, we could not observe TRPM6 homomer-like currents or Ca^{2+} uptake activities in placental trophoblasts. Even in a heterologous expression system in HEK293T cells, we could never observe TRPM6 homomer-like currents. To our knowledge, there were still no reports showing endogenous TRPM6 homomer, and only one vector construct can be used for the heterologous expression of TRPM6 homomer [18]. Indeed, TRPM6 homomer is not likely to be functional in physiological Mg^{2+} and ATP concentrations (Fig. 3e). Taken together, it is likely that TRPM6 is functional when it forms a complex with TRPM7. We hypothesize that TRPM6/TRPM7 is the molecular identity of the apical Ca^{2+} entry channels in the

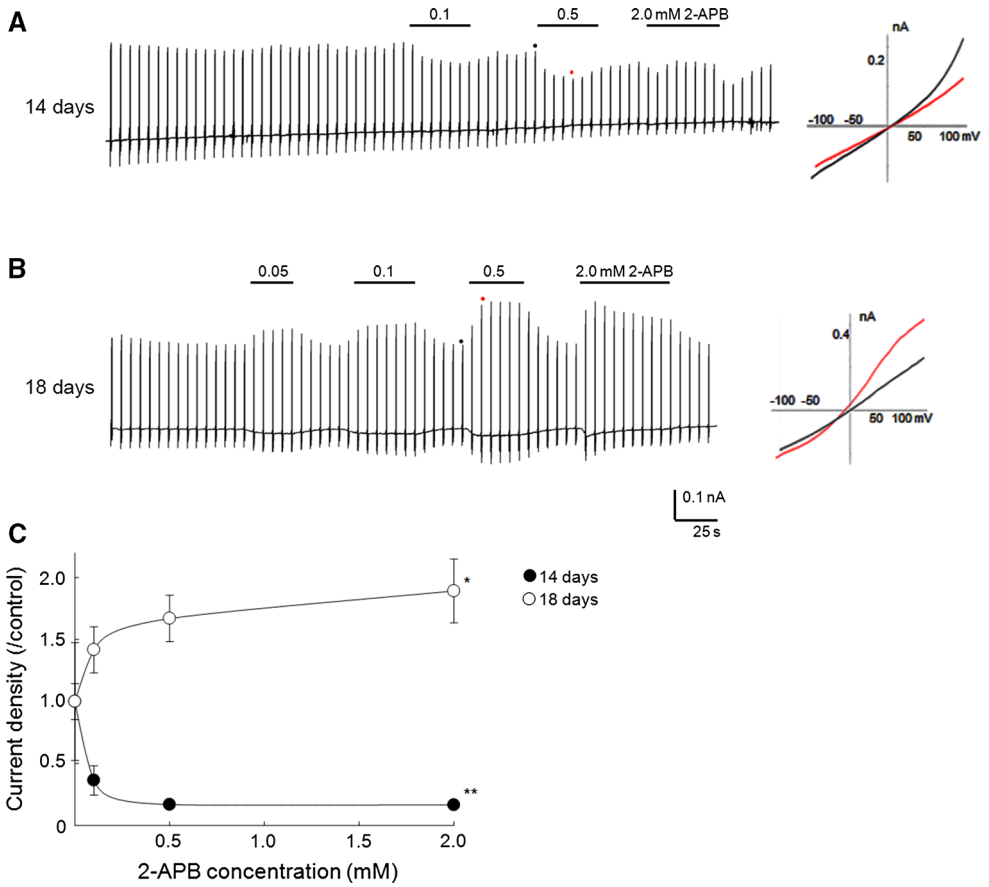

Fig. 4 Whole-cell patch-clamp recordings in mouse primary trophoblasts: **a** Representative time trace of membrane current in mouse primary trophoblasts at 14 days post-fertilization. Magnesium-inhibitable current (MIC) was observed ($n = 6$) and inhibited by 100 μM 2-APB. The outwardly rectifying current–voltage relationship is shown on the *right*. Data suggest that currents were derived from TRPM7 homomer. **b** Representative time trace of membrane current at 18 days post-fertilization, after initiation of fetal bone mineralization. The result indicated that 2-APB activated the membrane current in a dose-dependent manner ($n = 7$), which has been shown for TRPM6/TRPM7 heteromer in heterologous expression systems. These data suggest that currents were derived from TRPM6/TRPM7 heteromer. **c** Statistical analysis of the dose dependency of 2-APB at +110 mV. The decrease at 14 days and the increase at 18 days were statistically significant (**$p = 0.025$, $n = 7$; *$p = 0.047$, $n = 5$, one-way ANOVA with Bonferroni post hoc test). *Red and black dots* in the *traces* indicate the point at which I–V *curves* were generated

placenta in order to sustain the maternal–fetal Ca^{2+} transport for fetal bone mineralization.

It was reported that the Ca^{2+} uptake in human primary trophoblasts was inhibited by a broad TRP channel inhibitor ruthenium red and also by extracellular Mg^{2+} but not by voltage-gated Ca^{2+} channel inhibitors [12]. The authors speculated that the Ca^{2+} uptake was mediated by TRPV5 or TRPV6 or both. However, the expression of TRPV5 was restricted in the distal tubule cells of the kidney, and the TRPV5 expression in the placenta was extremely small throughout the placental development [6] (Fig. S1). In this study, we have found mRNA, protein, and functional expression of TRPM6/TRPM7 heteromer in mouse trophoblasts. Membrane currents were inhibited by extracellular Mg^{2+} and activated by 2-APB, as previously reported in exogenously expressed TRPM6/TRPM7 heteromer [15, 18] (Fig. 5). These results strongly support our above-mentioned hypothesis.

We performed Ca^{2+} imaging experiments to examine plasma membrane Ca^{2+} permeability in a physiological extracellular and intracellular divalent cation concentration. In this condition, if 2-APB could increase plasma membrane Ca^{2+} permeability by increasing TRPM6/TRPM7 activity, we could observe it as an increased intracellular Ca^{2+} concentration and actually this was the case (Fig. 3b–d). On the contrary, we could not observe any significant difference in the cells expressing TRPM6 or TRPM7 alone, most likely because these channels were blocked by physiological concentration of intracellular Mg^{2+} [18]. We speculate that this is the physiological meaning of TRPM6/TRPM7. Next, we performed whole-cell patch-clamp recordings to see how the endogenous

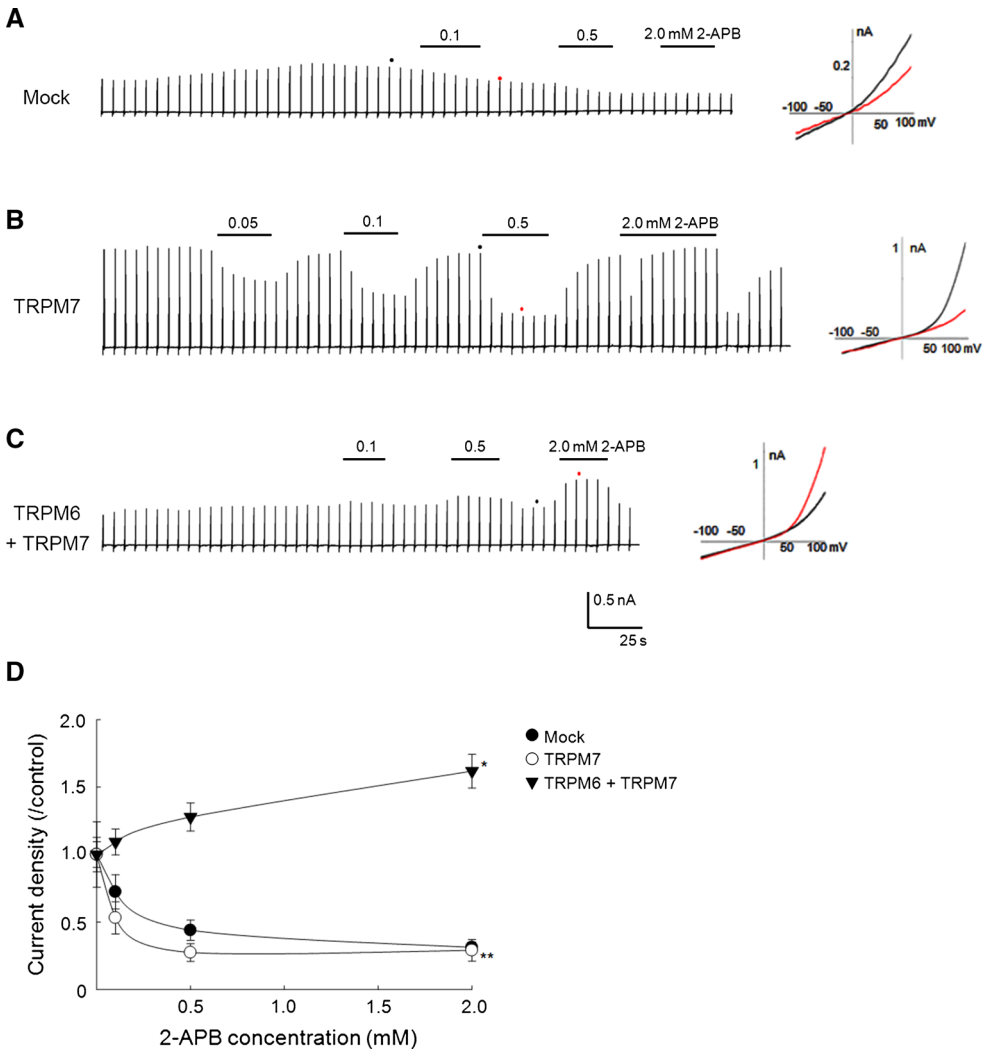

Fig. 5 Whole-cell patch-clamp recordings in HEK293T cells expressing TRPM7 alone or TRPM6 with TRPM7: **a** Representative time trace of membrane current from mock-transfected HEK293T cell. A small endogenous TRPM7-like currents were observed ($n = 5$). **b** Representative time trace from HEK293T cells expressing mouse TRPM7 alone. The current size was approximately ten-times larger compared to the endogenous currents, and these currents were inhibited by 0.1, 0.5, or 2.0 mM 2-APB ($n = 7$). The outwardly rectifying current–voltage relationship is shown on the *right*. **c** Representative time trace from HEK293T cells co-expressing mouse TRPM6 with TRPM7. The current was activated by 0.1, 0.5, or 2.0 mM 2-APB ($n = 7$). **d** Dose-dependent modification by the application of 2-APB at +110 mV. Currents from TRPM7 alone were inhibited, while currents of TRPM6 with TRPM7 were activated by 2-APB. These inhibitions or activations were statistically significant (**$p = 0.013$, $n = 4$; *$p = 0.002$, $n = 7$, one-way ANOVA with Bonferroni post hoc test). *Red* and *black dots* in the traces indicate the point at which I–V curves were generated

magnesium-inhibitable, TRPM7-like currents would change during late pregnancy, under extracellular and intracellular divalent cation-free conditions (intracellular ATP was used for a strong buffer for Mg^{2+}). This condition allowed us to see TRPM7-like currents more clearly, although this was not a very physiological one. In this case, we could observe a marked difference in membrane currents between 14 and 18 days post-fertilization as described in Fig. 4. The activation by 2-APB was observed only in positive potentials, most likely because we used divalent cation-free conditions. If we use physiological concentration of extracellular Ca^{2+}, there would be no currents in 14-day post-fertilization and it would be hard to see a difference in the aspect of TRPM7-like currents.

Regarding the plasma membrane Ca^{2+} permeability, we compared intracellular Ca^{2+} concentration among the mock-transfected cells and cells expressing TRPM6, TRPM7, or both, in a steady state. However, we could not find statistical difference of those. We hypothesized that it was because of the variation of the amount of intracellular Ca^{2+} buffers to avoid continuous increase of intracellular free Ca^{2+} concentration, which was known to be cytotoxic. Actually, in Western blotting we could confirm the cytotoxicity when TRPM6 was expressed with TRPM7

(Fig. 2a, lane 4 and 7). This result suggested that in a steady state, cells with higher intracellular free Ca^{2+} concentrations might be dead because of a Ca^{2+} overload, which might be other indirect evidence for an increase in plasma membrane Ca^{2+} permeability by TRPM6/TRPM7 heteromers.

It has been reported that *Trpm*6 or *Trpm*7 knockout mice (−/−) are embryonic lethal, and a statistically lower weight for *Trpm*6 −/− embryo compared to *Trpm*6 +/− or *Trpm*6 +/+ at 16.5, 17.5, and 18.5 days post-fertilization [20–22] was also found. Although there are so far no reports showing Ca^{2+} or Mg^{2+} composition in these embryos, these results suggest a defect of bone mineralization in *Trpm*6 −/− embryo due to a defect of the maternal–fetal Ca^{2+} and Mg^{2+} transport in the placenta. Future studies should focus on the contribution of TRPM6 in the maternal–fetal Ca^{2+} as well as Mg^{2+} transport. It has been shown that blood [Mg^{2+}] was significantly lower in adult *Trpm*6 +/− mice compared to *Trpm*6 +/+ mice, like in hypomagnesemic patients with TRPM6 mutations [23, 24]. Interestingly, it has also been shown that blood [Ca^{2+}] was lower under high Mg^{2+} conditions in adult *Trpm*6 +/− mice, suggesting that Mg^{2+} could compete with Ca^{2+} at the intestinal Ca^{2+} entry pathway [21], which was likely through a transcellular route under luminal low calcium condition. We speculate that there is a common Ca^{2+} and Mg^{2+} entry pathway in intestinal epithelium as well at least in part.

Intrauterine growth restriction (IUGR) is one of the major health problems worldwide. It has also been reported that a low birth weight resulting from IUGR might be a risk factor for other diseases such as diabetes and hypertension after growth [25]. Although poor maternal–fetal transport of nutrition including Ca^{2+} might be one of the promising causes of IUGR [26], in most cases the molecular mechanisms of IUGR is still not understood. In human placenta, syncytiotrophoblasts play a role in the maternal–fetal nutrient transport including Ca^{2+}. Based on our results, we propose that TRPM6 plays a role in the maternal–fetal Ca^{2+} transport in human syncytiotrophoblasts cooperatively with TRPV6. Smaller embryonic weight in *Trpm*6 −/− [20] as well as *Trpv*6 −/− [6] might support this hypothesis. In *Trpv*6 −/− mice, the maternal–fetal Ca^{2+} transport still remained 60 % [6], probably due to the compensatory role of TRPM6 in terms of Ca^{2+} transport. One can speculate that TRPM6/TRPM7 heteromer might be important for balky transport of divalent cations, whereas TRPV6 might be critical for more Ca^{2+}-selective transport for a fine tuning of Ca^{2+} level. The association between these genes encoding these channels and human diseases including IUGR would facilitate the understanding of the functional significance of these channels.

In summary, we found that TRPM6 is functionally expressed in mouse placental trophoblasts, most likely with TRPM7. The spatio-temporal expression pattern suggests that TRPM6 plays a role in the maternal–fetal Ca^{2+} transport in order to sustain fetal bone mineralization. Future studies need to focus on the molecular mechanism of regulation of the maternal–fetal transport by fetal demands.

Acknowledgments We thank members of the Division of Cell Signaling, Okazaki Institute for Integrative Bioscience (National Institute for Physiological Sciences, Japan) for scientific discussion and technical assistance. This work was supported by a Grant-in-Aid for Scientific Research to YS from the Ministry of Education, Culture, Sports, Science and Technology in Japan.

Compliance with ethical standards

Conflict of interest The authors declare that they have no conflicts of interest.

References

1. Pitkin RM (1985) Calcium metabolism in pregnancy and the perinatal period: a review. Am J Obstet Gynecol 151:99–109
2. Stulc J (1997) Placental transfer of inorganic ions and water. Physiol Rev 77:805–836
3. Twardock AR (1967) Placental transfer of calcium and strontium in the guinea pig. Am J Physiol 213:837–842
4. Hoenderop JG, Nilius B, Bindels RJ (2005) Calcium absorption across epithelia. Physiol Rev 85:373–422
5. Suzuki Y, Landowski CP, Hediger MA (2008) Mechanisms and regulation of epithelial Ca2+ absorption in health and disease. Annu Rev Physiol 70:257–271
6. Suzuki Y, Kovacs CS, Takanaga H, Peng JB, Landowski CP, Hediger MA (2008) Calcium channel TRPV6 is involved in murine maternal–fetal calcium transport. J Bone Miner Res 23:1249–1256
7. Mizuno H, Suzuki Y, Watanabe M, Sokabe T, Yamamoto T, Hattori R et al (2014) Potential role of transient receptor potential (TRP) channels in bladder cancer cells. J Physiol Sci 64:305–314
8. Miyamoto T, Mochizuki T, Nakagomi H, Kira S, Watanabe M, Takayama Y et al (2014) Functional role for Piezo1 in stretch-evoked Ca(2)(+) influx and ATP release in urothelial cell cultures. J Biol Chem 289:16565–16575
9. Watanabe M, Suzuki Y, Uchida K, Miyazaki N, Murata K, Matsumoto S et al (2015) Trpm7 Protein Contributes to Intercellular Junction Formation in Mouse Urothelium. J Biol Chem 290:29882–29892
10. Yamaguchi M, Ogren L, Endo H, Thordarson G, Kensinger R, Talamantes F (1992) Epidermal growth factor stimulates mouse placental lactogen I but inhibits mouse placental lactogen II secretion in vitro. Proc Natl Acad Sci USA 89:11396–11400
11. Loh NY, Bentley L, Dimke H, Verkaart S, Tammaro P, Gorvin CM et al (2013) Autosomal dominant hypercalciuria in a mouse model due to a mutation of the epithelial calcium channel, TRPV5. PLoS ONE 8:e55412
12. Moreau R, Daoud G, Bernatchez R, Simoneau L, Masse A, Lafond J (2002) Calcium uptake and calcium transporter expression by trophoblast cells from human term placenta. Biochim Biophys Acta 1564:325–332
13. Sommer B, Bickel M, Hofstetter W, Wetterwald A (1996) Expression of matrix proteins during the development of mineralized tissues. Bone 19:371–380

14. Nilius B, Weidema F, Prenen J, Hoenderop JG, Vennekens R, Hoefs S et al (2003) The carboxyl terminus of the epithelial Ca(2+) channel ECaC1 is involved in Ca(2+)-dependent inactivation. Pflugers Arch 445:584–588
15. Li M, Jiang J, Yue L (2006) Functional characterization of homo- and heteromeric channel kinases TRPM6 and TRPM7. J Gen Physiol 127:525–537
16. Neeper MP, Liu Y, Hutchinson TL, Wang Y, Flores CM, Qin N (2007) Activation properties of heterologously expressed mammalian TRPV2: evidence for species dependence. J Biol Chem 282:15894–15902
17. Kovacs G, Montalbetti N, Simonin A, Danko T, Balazs B, Zsembery A et al (2012) Inhibition of the human epithelial calcium channel TRPV6 by 2-aminoethoxydiphenyl borate (2-APB). Cell Calcium 52:468–480
18. Zhang Z, Yu H, Huang J, Faouzi M, Schmitz C, Penner R et al (2014) The TRPM6 kinase domain determines the Mg.ATP sensitivity of TRPM7/M6 heteromeric ion channels. J Biol Chem 289:5217–5227
19. Schmitz C, Dorovkov MV, Zhao X, Davenport BJ, Ryazanov AG, Perraud AL (2005) The channel kinases TRPM6 and TRPM7 are functionally nonredundant. J Biol Chem 280:37763–37771
20. Walder RY, Yang B, Stokes JB, Kirby PA, Cao X, Shi P et al (2009) Mice defective in Trpm6 show embryonic mortality and neural tube defects. Hum Mol Genet 18:4367–4375
21. Woudenberg-Vrenken TE, Sukinta A, van der Kemp AW, Bindels RJ, Hoenderop JG (2011) Transient receptor potential melastatin 6 knockout mice are lethal whereas heterozygous deletion results in mild hypomagnesemia. Nephron Physiol 117:p11–p19
22. Jin J, Desai BN, Navarro B, Donovan A, Andrews NC, Clapham DE (2008) Deletion of Trpm7 disrupts embryonic development and thymopoiesis without altering Mg2+ homeostasis. Science 322:756–760
23. Schlingmann KP, Weber S, Peters M, Niemann Nejsum L, Vitzthum H, Klingel K et al (2002) Hypomagnesemia with secondary hypocalcemia is caused by mutations in TRPM6, a new member of the TRPM gene family. Nat Genet 31:166–170
24. Walder RY, Landau D, Meyer P, Shalev H, Tsolia M, Borochowitz Z et al (2002) Mutation of TRPM6 causes familial hypomagnesemia with secondary hypocalcemia. Nat Genet 31:171–174
25. Morton JS, Cooke CL, Davidge ST (2016) In utero origins of hypertension: mechanisms and targets for therapy. Physiol Rev 96:549–603
26. Baczyk D, Kingdom JC, Uhlen P (2011) Calcium signaling in placenta. Cell Calcium 49:350–356